

# Direct Power Control Based Matrix Converter and Its Operation Characteristics

Toshihiko Noguchi, Somei Nakatomi, and Daisuke Takeuchi

Nagaoka University of Technology  
 1603-1 Kamitomioka, Nagaoka 940-2188, JAPAN  
 tnoguchi@vos.nagaokaut.ac.jp

**Abstract** – This paper proposes a novel control strategy of a matrix converter, which features direct instantaneous-active- and reactive-power control of the converter. The power can directly be regulated by selecting an optimum switching state with a relay (bang-bang) control algorithm; thus an ultimately high-speed response of the power control is achieved. A theoretical aspect of the control is discussed, and some computer simulation results are presented to confirm the basic controllability of the technique. In addition, several operation characteristics are examined through experimental tests, using a 1.5-kW prototype. The maximum efficiency and total input power factor of the experimental setup were 95.4 % and 99.9 % at 1.5-kW load with 30-Hz output frequency, respectively. Also, the total harmonic distortion of the input current was 5.9 % at the rated load condition. These results prove feasibility and effectiveness of the proposed strategy.

## I. INTRODUCTION

In general, an AC/DC/AC power conversion is extensively used in a variety of power system applications, industry applications, transportation systems, and etc., which requires a rectifier, a DC bus, and an inverter to obtain arbitrary AC power from a utility power source. Since two-stage power conversion is indispensable in such conventional systems, however, total power conversion efficiency from the utility power source to a load is normally around 90 % at most and it is rather difficult to improve the efficiency higher than 95 %. Furthermore, the conventional system requires a bulky energy-buffering device such as an electrolytic capacitor to smooth DC bus voltage, which prevents physical size reduction and longer product life of the whole apparatus. In recent years, therefore, matrix converters have intensively been studied and many researchers have published a numerous number of papers on the matrix converters because it makes a direct AC/AC power conversion possible without any energy-buffering devices.

The authors have been investigating a direct power control (DPC) strategy of power converters and its application to various power conversion systems. This strategy features relay (bang-bang) control of instantaneous active and reactive power, which is accomplished by a direct selection of an optimum switching state of the power converter. The DPC system requires none of a current minor loop, rotational coordinate transformation, and a linear regulator such as a PI element to control the power converter. Therefore, the strategy allows an ultimately high-speed power control response, which leads to minimization of the energy-buffering device, and is likely suitable to control of the matrix converter

because it requires an extremely high-speed response in power management due to its particular circuit topology with no energy-buffering devices.

This paper describes the DPC strategy applied to the matrix converter, and presents the system configuration and performances, which includes a theoretical aspect of the proposed control strategy, a feasibility study through computer simulations and real performance evaluation with a 1.5-kW experimental setup.

## II. SYSTEM CONFIGURATION AND CONTROL ALGORITHM OF DPC BASED MATRIX CONVERTER

### A. Switching State of Matrix Converter

The proposed DPC based matrix converter employs a virtual AC/DC/AC power conversion approach to determine the switching state of the matrix converter at every moment. This approach divides the matrix converter into two parts, i.e., a virtual front-end AC/DC rectifier and a virtual DC/AC inverter, and synthesizes the switching state of the matrix converter from the both switching states of the virtual rectifier and the virtual inverter.

Fig. 1 illustrates a matrix converter, where  $v_a$ ,  $v_b$ , and  $v_c$  are input voltages from the utility power source and  $v_u$ ,  $v_v$ , and  $v_w$  are output voltages to the load. The relationship between the input voltages and the output voltages can be expressed as (1), using a set of switching states of the matrix converter.

$$\begin{bmatrix} v_u \\ v_v \\ v_w \end{bmatrix} = \begin{bmatrix} S_{au} & S_{bu} & S_{cu} \\ S_{av} & S_{bv} & S_{cv} \\ S_{aw} & S_{bw} & S_{cw} \end{bmatrix} \begin{bmatrix} v_a \\ v_b \\ v_c \end{bmatrix} \dots\dots\dots (1)$$

In the above equation, each switching state takes a value of either “1” or “0”, according to the “ON” or “OFF” state of each bidirectional device, respectively.

On the other hand, an AC/DC/AC power conversion system composed with a three-phase PWM rectifier and a three-phase

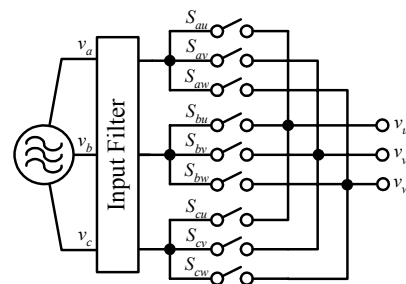


Fig. 1. Simplified circuit diagram of matrix converter.

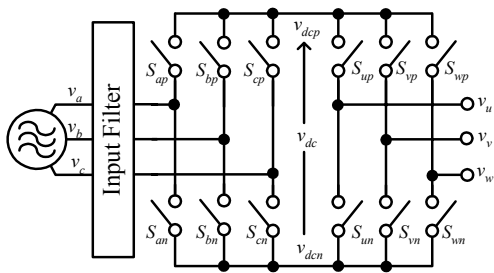


Fig. 2. AC/DC/AC power conversion system.

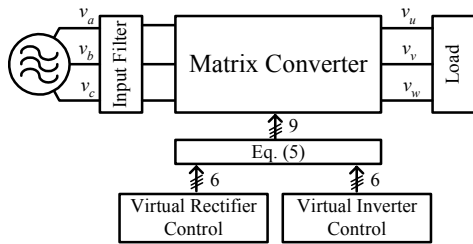


Fig. 3. Virtual AC/DC/AC conversion based matrix converter control.

PWM inverter is depicted in Fig. 2, where  $v_{dcp}$  and  $v_{dcn}$  represent a high-side voltage and a low-side voltage of the rectifier output with respect to a neutral point of the DC bus. Therefore, the output voltages of the rectifier are expressed as (2), using its set of switching states.

$$\begin{bmatrix} v_{dcp} \\ v_{dcn} \end{bmatrix} = \begin{bmatrix} S_{ap} & S_{bp} & S_{cp} \\ S_{an} & S_{bn} & S_{cn} \end{bmatrix} \begin{bmatrix} v_a \\ v_b \\ v_c \end{bmatrix} \dots \dots \dots (2)$$

In a similar manner, the relationship between the output of the inverter and the DC bus voltages can mathematically be described as (3).

$$\begin{bmatrix} v_u \\ v_v \\ v_w \end{bmatrix} = \begin{bmatrix} S_{up} & S_{un} \\ S_{vp} & S_{vn} \\ S_{wp} & S_{wn} \end{bmatrix} \begin{bmatrix} v_{dcp} \\ v_{dcn} \end{bmatrix} \dots \dots \dots (3)$$

By substituting (2) into the above equation, therefore, the output AC voltages to the load can be expressed as a function of the input AC voltages from the utility power source, using a product of two sets of switching state matrices as follows:

$$\begin{bmatrix} v_u \\ v_v \\ v_w \end{bmatrix} = \begin{bmatrix} S_{up} & S_{un} \\ S_{vp} & S_{vn} \\ S_{wp} & S_{wn} \end{bmatrix} \begin{bmatrix} S_{ap} & S_{bp} & S_{cp} \\ S_{an} & S_{bn} & S_{cn} \end{bmatrix} \begin{bmatrix} v_a \\ v_b \\ v_c \end{bmatrix} \dots \dots \dots (4)$$

In order to obtain the same input-and-output relationship as shown in (4) with that of the matrix converter expressed by (1), the following equation must be held among the switching state matrices:

$$\begin{bmatrix} S_{au} & S_{bu} & S_{cu} \\ S_{av} & S_{bv} & S_{cv} \\ S_{aw} & S_{bw} & S_{cw} \end{bmatrix} = \begin{bmatrix} S_{up} & S_{un} \\ S_{vp} & S_{vn} \\ S_{wp} & S_{wn} \end{bmatrix} \begin{bmatrix} S_{ap} & S_{bp} & S_{cp} \\ S_{an} & S_{bn} & S_{cn} \end{bmatrix} \dots \dots \dots (5)$$

In the matrix converter shown in Fig. 1, it is necessary never

to have short-circuit among power source terminals nor open-circuit at the output terminals because the load is regarded as an inductive component. Therefore, a front end of the virtual AC/DC/AC power conversion system is necessarily a current-source type rectifier, while an output stage of the virtual AC/DC/AC power conversion system has to be a voltage-source type inverter. The switching state of the actual matrix converter can be determined by (5) as if there are two independent conventional power converters to be controlled, i.e., the virtual current-source PWM rectifier and the virtual voltage-source PWM inverter. Fig. 3 illustrates a block diagram of the matrix converter controller on the basis of the virtual AC/DC/AC power conversion system. In this paper, a DPC based current-source PWM rectifier and a current-controlled voltage-source PWM inverter are introduced to satisfy the above requirements and to determine the switching state of the matrix converter at every moment.

*B. Control of DPC Based Virtual Current-Source PWM Rectifier*

The DPC technique is applied to the virtual current-source PWM rectifier because of its extremely high-speed response in power management. Fig. 4 indicates a block diagram of the direct power controller. As shown in the figure, instantaneous active power  $P$  and instantaneous reactive power  $Q$  are calculated from the voltages and the currents of the utility power source.

$$\begin{bmatrix} P \\ Q \end{bmatrix} = \begin{bmatrix} v_\alpha & v_\beta \\ v_\beta & -v_\alpha \end{bmatrix} \begin{bmatrix} i_\alpha \\ i_\beta \end{bmatrix} \dots \dots \dots (6)$$

where  $v_\alpha$  and  $v_\beta$  are two-phase voltages and  $i_\alpha$  and  $i_\beta$  are two-phase currents obtained by the following coordinate transformations:

$$\begin{bmatrix} v_\alpha \\ v_\beta \end{bmatrix} = \frac{\sqrt{2}}{\sqrt{3}} \begin{bmatrix} 1 & -1/2 & -1/2 \\ 0 & \sqrt{3}/2 & -\sqrt{3}/2 \end{bmatrix} \begin{bmatrix} v_a \\ v_b \\ v_c \end{bmatrix} \dots \dots \dots (6a)$$

$$\begin{bmatrix} i_\alpha \\ i_\beta \end{bmatrix} = \frac{\sqrt{2}}{\sqrt{3}} \begin{bmatrix} 1 & -1/2 & -1/2 \\ 0 & \sqrt{3}/2 & -\sqrt{3}/2 \end{bmatrix} \begin{bmatrix} i_a \\ i_b \\ i_c \end{bmatrix} \dots \dots \dots (6b)$$

In general, a current-source PWM rectifier requires an input LC filter, which may cause current waveform distortions due to the LC resonance. Therefore, it is necessary to dump the LC resonance with a power feedback compensation, which is composed by differential elements  $k_d$ . This compensator adds a dumping factor to the transfer function between the AC power source and the DC bus of the virtual PWM rectifier.

The instantaneous active power command  $P^*$  is obtained from a product between the load power  $P_L$  and a normalized virtual DC bus voltage as shown in (7). The load power  $P_L$  can simply be obtained from voltage commands and current feedback signals in the virtual inverter, while the normalized virtual DC bus voltage is derived from the detected power-source voltages.

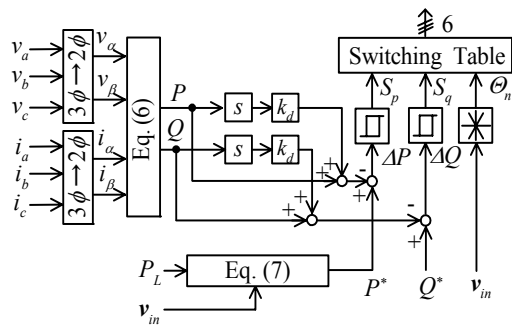


Fig. 4. Block diagram of direct power controller for virtual current-source PWM rectifier.

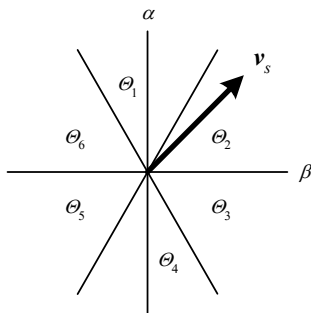


Fig. 5. Quantized phase of power-source voltage vector.

$S_p$	$S_q$	$\theta_1$	$\theta_2$	$\theta_3$	$\theta_4$	$\theta_5$	$\theta_6$
1	0	PON	OPN	NPO	NOP	ONP	PNO
1	1	PNO	PON	OPN	NPO	NOP	ONP
0	0	SOO	OOS	OSO	SOO	OOS	OSO
0	1	ONP	PNO	PON	OPN	NPO	NOP

Fig. 6. Optimum switching state table and comparators for quantization.

$$P^* = P_L \max \left\{ \begin{bmatrix} 1 & -1 & 0 \\ 0 & 1 & -1 \\ -1 & 0 & 1 \end{bmatrix} \begin{bmatrix} \cos \omega t \\ \cos(\omega t - 2\pi/3) \\ \cos(\omega t - 4\pi/3) \end{bmatrix} \right\} \dots \dots \dots (7)$$

On the other hand, the instantaneous reactive power command  $Q^*$  is provided from the outside of the controller, and is normally set at zero to achieve a unity total power factor operation.

Control errors  $\Delta P = P^* - P$  and  $\Delta Q = Q^* - Q$  are quantized with hysteresis comparators, generating signals  $S_p$  and  $S_q$ . A phase angle of the power-source voltage vector is also quantized to 6 sectors  $\theta_n$ , as shown in Fig. 5, where  $\alpha$ -axis and  $\beta$ -axis denote real and imaginary parts of the vector, respectively. The quantized phase  $\theta_n$  is mathematically

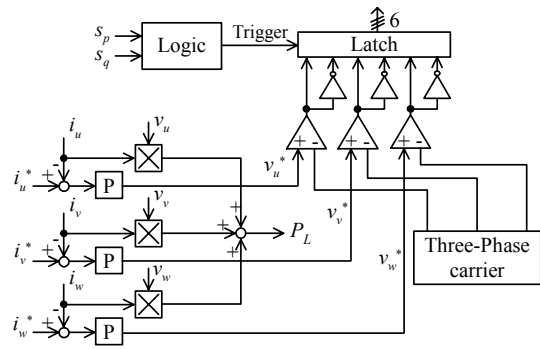


Fig. 7. Block diagram of current controller for virtual voltage-source PWM inverter.

expressed as

$$\frac{\pi}{6}(2n-3) \leq \theta_n < \frac{\pi}{6}(2n-1) \quad \because n=1, 2, \dots, 6. \dots \dots \dots (8)$$

By using the quantized signals  $S_p$ ,  $S_q$  and  $\theta_n$ , the most appropriate switching state of the virtual PWM rectifier is uniquely determined to restrict the control errors  $\Delta P$  and  $\Delta Q$  within the predetermined hysteresis bandwidth. In order to achieve this relay control operation, an optimum switching state table shown in Fig. 6 is employed to select a unique optimum switching state of the virtual PWM rectifier, according to a combination of the quantized signals  $S_p$ ,  $S_q$  and  $\theta_n$ . In the table, a switching state “P” indicates that high side device is turned on and that low side device is turned off, and “N” indicates vice versa. Another switching state “O” corresponds to a state that both of high- and low-side devices in a specific leg are simultaneously turned off, while “S” means a short circuit situation by turning on the high- and the low-side devices in one of the three legs at the same time.

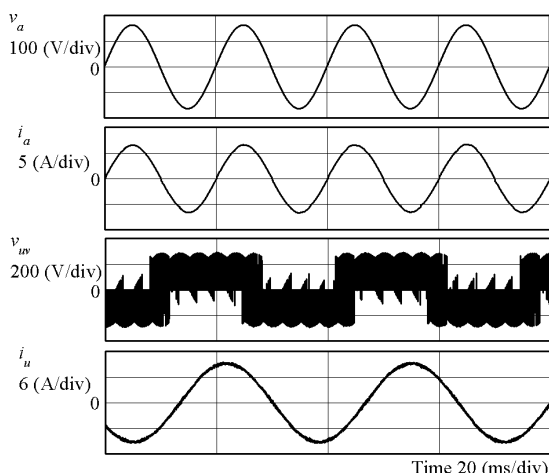
Since the DPC system is in principle based on a relay control algorithm, it is significant to investigate relationship between the switching state and behaviours of the instantaneous active and reactive power, i.e., time derivatives  $dP/dt$  and  $dQ/dt$  derived as functions of the switching state of the virtual PWM rectifier as follows:

$$\frac{dP}{dt} = \frac{I_{rms}}{C_f} \left[ -3I_{rms} + \sqrt{2}I_{dc} \left\{ (S_u - \frac{S_v}{2} - \frac{S_w}{2}) \cos \theta + \frac{\sqrt{3}}{2} (S_v - S_w) \sin \theta \right\} \right], \text{ and } \dots \dots (9)$$

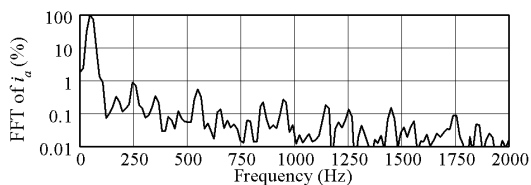
$$\frac{dQ}{dt} = \frac{\sqrt{2}I_{rms}I_{DC}}{C_f} \left\{ -\frac{\sqrt{3}}{2} (S_v - S_w) \cos \theta + (S_u - \frac{S_v}{2} - \frac{S_w}{2}) \sin \theta \right\} \dots \dots \dots (10)$$

In the above equations,  $I_{rms}$ ,  $I_{DC}$ ,  $\theta$ , and  $C_f$  are an rms value of the power source current vector, virtual DC bus current, an argument of the power source voltage vector and a capacitance of the LC filter, respectively.

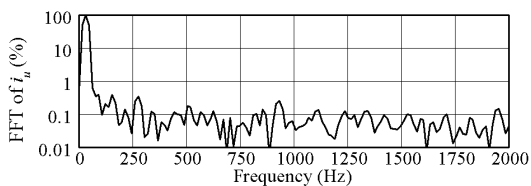
According to polarities of the time derivatives  $dP/dt$  and



(a) Power source voltage, input current, output voltage, and load current waveforms.



(b) Frequency spectrum of input current.



(c) Frequency spectrum of load current.

Fig. 8. Simulation result at 30-Hz and 1.5-kW output.

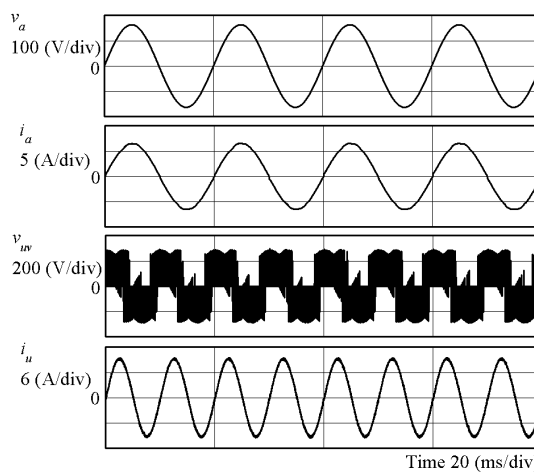
TABLE I ELECTRIC PARAMETERS OF POWER CIRCUIT.

Power source voltage	200 V, 50 Hz
Input filter inductance $L_f$	2.7 mH
Input filter capacitance $C_f$	20 $\mu$ F
Load	12.5 $\Omega$ , 3.7 mH
Reactive power command	0 var

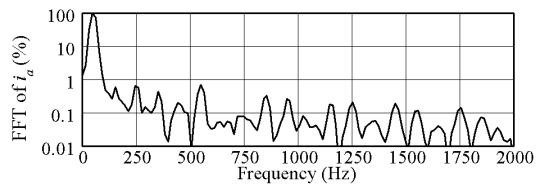
$dQ/dt$  solved as (9) and (10), one of the switching states of the virtual PWM rectifier can uniquely be determined to restrict the control errors  $\Delta P$  and  $\Delta Q$  within the hysteresis bandwidth, which leads to determination of the contents of the optimum switching state table.

### C. Control of Virtual Voltage-Source PWM Inverter

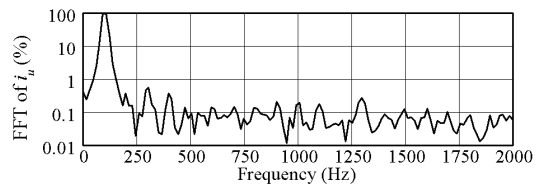
Fig. 7 shows a block diagram of a controller for the virtual voltage-source PWM inverter with current minor loops. As shown here, the inverter output voltage commands  $v_u^*$ ,  $v_v^*$  and  $v_w^*$  are obtained from control errors between the current feedback signals  $i_u$ ,  $i_v$ ,  $i_w$  and their commands  $i_u^*$ ,  $i_v^*$ ,  $i_w^*$ . The voltage commands are converted to PWM signals with a sub-harmonic modulation technique, where three-phase triangular-wave signals are employed as a PWM carrier. The



(a) Power source voltage, input current, output voltage, and load current waveforms.



(b) Frequency spectrum of input current.



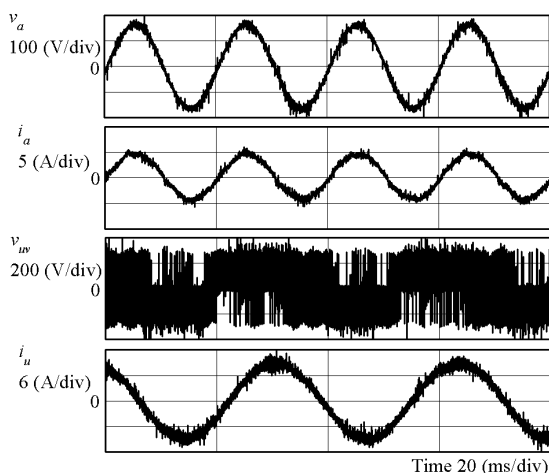
(c) Frequency spectrum of load current.

Fig. 9. Simulation result at 100-Hz and 1.5-kW output.

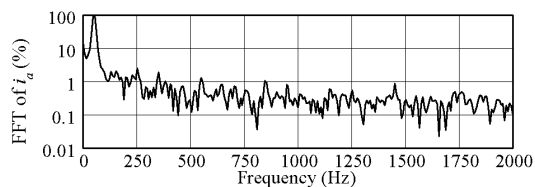
PWM technique using the three-phase carrier does not generate zero-voltage vectors that cause a freewheeling mode among the three-phase load terminals; hence this approach guarantees continuity of the virtual DC bus current. If there is an interruption in the virtual DC bus current for any reasons, a detrimental waveform distortion will appear in the input current of the virtual PWM rectifier. To the contrary, while the virtual PWM rectifier generates a zero-current vector by making a short circuit across the virtual DC bus (a freewheeling mode), the virtual DC bus voltage becomes zero, which detrimentally affects the output of the virtual PWM inverter. To minimize an effect of the interference, therefore, an exceptional treatment is given to the optimum switching state table and the virtual PWM inverter is prohibited to change its switching state when the short circuit occurs across the virtual DC bus. This special restriction mode is easily detected from the control signals  $S_p$  and  $S_q$  of the virtual PWM rectifier.

As described in the previous section, the load power  $P_L$  is calculated to provide the virtual PWM rectifier with the instantaneous active power command  $P^*$  as shown in (11).

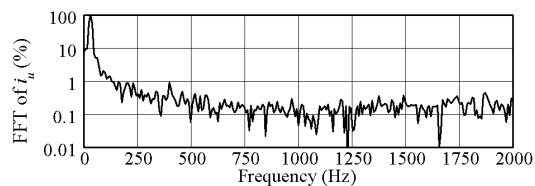
$$P_L = v_u^* i_u + v_v^* i_v + v_w^* i_w \dots \dots \dots (11)$$



(a) Power source voltage, input current, output voltage, and load current waveforms.



(b) Frequency spectrum of input current.



(c) Frequency spectrum of load current.

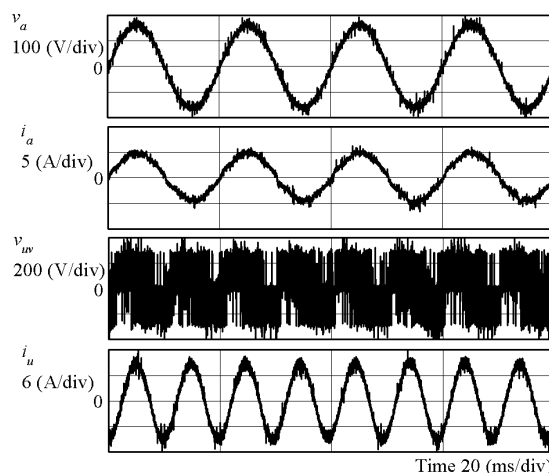
Fig. 10. Experimental result at 30-Hz and 1.5-kW output.

### III. COMPUTER SIMULATION RESULTS

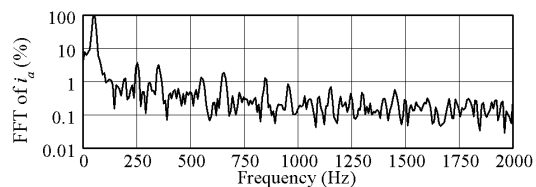
Computer simulations were conducted with PSIM software to investigate the basic operation performance of the proposed strategy. The electric parameters of a power circuit used in the simulations are listed in TABLE I. Fig. 8 and Fig. 9 show operation waveforms and frequency spectra of the input and the output currents at 30 Hz output and 100 Hz output, respectively. In both cases, the load was 1.5 kW and the reactive power command was 0 var. As is indicated in the figures, the unity total input power factor operation is achieved at the grid frequency of 50 Hz, and sinusoidal input current waveforms are confirmed in both test conditions. In addition, the sinusoidal output currents are provided to the load at both commanded frequencies of 30 Hz and 100 Hz as well. The FFT analysis results of the input and the output currents indicate that most of the harmonics is less than 1%, which demonstrates excellent performance of the proposed strategy.

### IV. EXPERIMENTAL SETUP AND RESULTS

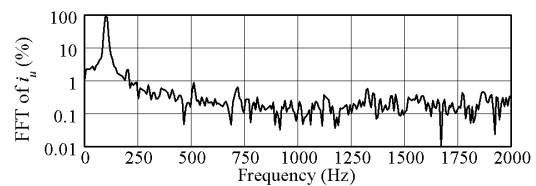
A 1.5 kW prototype was developed to confirm



(a) Power source voltage, input current, output voltage, and load current waveforms.



(b) Frequency spectrum of input current.



(c) Frequency spectrum of load current.

Fig. 11. Experimental result at 100-Hz and 1.5-kW output.

experimentally feasibility and effectiveness of the DPC based control of the matrix converter. The prototype has the same specifications and parameters used in the computer simulations. Fig. 10 and Fig. 11 show experimental results obtained under the identical test conditions as those of the simulations. As can be seen in these figures, the input current is in phase with the power source voltage and is controlled to be sinusoidal in both cases of the 30 Hz output and the 100 Hz output. The measured frequency spectra of the input current include slightly larger harmonics than those of the simulation results, but few conspicuous peaks are observed over the wide range of frequency band in both cases. On the other hand, the output currents are well controlled at the commanded frequency of 30 Hz and 100 Hz and have quite low harmonic spectra less than 1%, which is confirmed by the current waveforms as well as the FFT analysis results.

Fig. 12 and Fig. 13 show characteristics of the total input power factor and the total efficiency, respectively. The maximum total input power factor was 99.9% and the maximum total efficiency was 95.4% under the conditions of both 30-Hz and 100 Hz output frequencies and 1.5-kW load. The frequency change of the output currents does not affect very seriously on the overall operation performance. Fig. 14 represents the total harmonic distortion of the output currents,

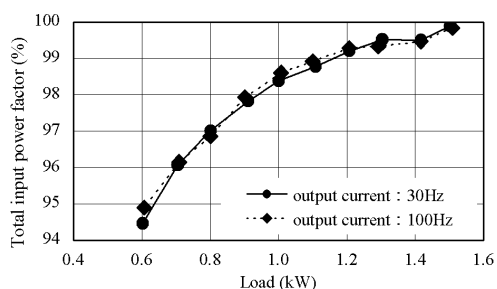


Fig. 12. Characteristics of total input power factor.

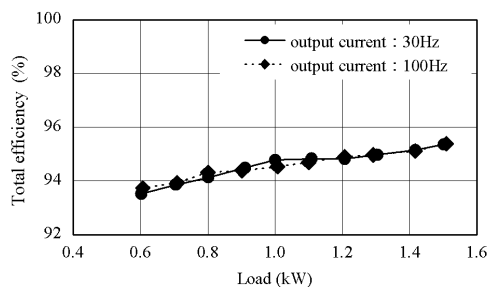


Fig. 13. Characteristics of total efficiency.

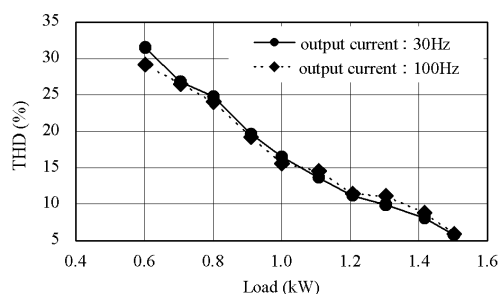


Fig. 14. Characteristics of total harmonic distortion of input current.

which show the minimum value of 5.9 % was measured at 1.5-kW rated load. However, the total harmonic distortion characteristics become worse up to approximately 30 % as the load power is reduced. Further performance improvement is expected in the light-load range in the future works.

## V. CONCLUSION

This paper proposed a novel control strategy of a matrix converter, which featured direct control of the instantaneous active and reactive power on the basis of a relay (bang-bang) control algorithm. A theoretical aspect of the proposed technique was discussed prior to the computer simulations and experimental tests. By using a 1.5-kW experimental set up, excellent controllability of the input current was confirmed, resulting in 99.9-% total input power factor and low input harmonics less than 1 % regardless of the output frequency. Also, well-controlled output currents were observed at the desired frequency independently of the fixed utility power source frequency. As a result, the maximum efficiency of 95.4 % was accomplished at the rated load of 1.5 kW through the experiments. Even assuming that both of the conventional PWM rectifier and the PWM inverter have 95 % efficiency,

the total efficiency of such an AC/DC/AC power conversion system can achieve nearly 90-% efficiency at most. From the viewpoint of the total efficiency between the AC power source and the AC load, however, the proposed system has a great advantage over the conventional system, which is the most attractive point.

## VI. REFERENCES

- [1] L. Huber, and D. Borjevic, "Space Vector Modulated Three-Phase to Three-Phase Matrix Converter with Input Power Factor Correction," *IEEE Trans on Ind. Appl.*, vol. 31, no. 6, 1995, p.p. 1234-1245.
- [2] D. Casadei, G. Serra, and A. Tani, "The Use of Matrix Converter in Direct Torque Control of Induction Machines," *IEEE Trans. on Ind. Elec.*, vol. 48, no. 6, 2001, p.p. 1057-1064.
- [3] R. Itoh, and I. Takahashi, "Decoupling Control of Input and Reactive Power of the Matrix Converter," *IEEJ Proc. Tech. Meet., SPC-01-121*, 2001.
- [4] D. Takeuchi, A. Sato, and T. Noguchi, "New Control Strategy of Matrix Converter Based on Direct Power Control," *IEEJ Proc. Ind. App. Soc. Conf.*, vol. 1, 2004, p.p. 309-312.
- [5] L. Helle, K. B. Larsen, A. H. Jogensen, S. M. Nielsen, and F. Blaabjerg, "Evaluation of Modulation Schemes for Three-Phase to Three-Phase Matrix Converters," *IEEE Trans. on Ind. Elec.*, vol. 51, no. 1, 2004, p.p. 158-171.
- [6] P. W. Wheeler, J. Rodrigues, J. C. Clare, L. Empringham, and A. Weinstein, "Matrix Converters: A Technology Review," *IEEE Trans. on Ind. Elec.*, vol. 49, no. 2, 2002, p.p. 276-288.
- [7] P. Mutschler, and M. Marcks, "A Direct Control Method for Matrix Converters," *IEEE Trans. on Ind. Elec.*, vol. 49, no. 2, 2002, p.p. 362-369.
- [8] J. Itoh, I. Sato, H. Ohguchi, K. Sato, A. Odaka, and N. Eguchi, "A Control Method for the Matrix Converter Based on Virtual AC/DC/AC Converter Using Carrier Comparison Method," *IEEJ Trans on Ind. App.*, vol. 124-D, no. 5, 2004, p.p. 457-463.
- [9] S. Muller, U. Ammann, and S. Rees, "New Time-Discrete Modulation Scheme for Matrix Converters," *IEEE Trans. on Ind. Elec.*, vol. 52, no. 6, 2005, p.p. 1607-1615.
- [10] H. Hara, E. Yamamoto, J. K. Kang, and T. Kume, "Improvement of Output Voltage Control Performance for Low-Speed Operation of Matrix Converter," *IEEE Trans on Power Elec.*, vol. 20, no. 6, 2005, p.p. 1372-1378.
- [11] T. Noguchi, A. Sato, and D. Takeuchi, "Minimization of Smoothing Capacitor and Operation Characteristics under Unbalanced Power Source of Direct-Power-Controlled PWM Rectifier," *IEEJ Trans. on Ind. App.*, vol. 126-D, no. 2, 2006, p.p. 103-108.
- [12] C. Klumpner, F. Blaabjerg, I. Boldea, and P. Nielsen, "New Modulation Method for Matrix Converters," *IEEE Trans on Ind. Appl.*, vol. 42, no. 3, 2006, p.p. 797-806.